OFDM Signal Detection in Doubly Selective Channels with Blockwise Whitening of Residual Intercarrier Interference and Noise

Hai-wei Wang, David W. Lin, *Senior Member, IEEE*, and Tzu-Hsien Sang, *Member, IEEE*

***Abstract*—Orthogonal frequency-division multiplexing (OFDM) is a popular broadband wireless transmission technique, but its performance can suffer severely from the intercarrier interference (ICI) induced by fast channel variation arising from high-speed motion. Existing ICI countermeasures usually address a few dominant ICI terms only and treat the residual similar to white noise. We show that the residual ICI has high normalized autocorrelation and that this normalized autocorrelation is insensitive to the multipath channel profile as well as a variety of other system and channel conditions. Consequently, the residual ICI plus noise can be whitened in a nearly channel-independent manner, leading to significantly improved detection performance. Simulation results confirm the theoretical analysis. In particular, they show that the proposed technique can significantly lower the ICI-induced error floor in maximum-likelihood sequence estimation (MLSE) designed to address a few dominant ICI terms.**

***Index Terms*—Doppler spread, intercarrier interference (ICI), maximum-likelihood sequence estimation (MLSE), orthogonal frequency-division multiplexing (OFDM), time-varying channels.**

I. Introduction

ORTHOGONAL frequency-division multiplexing (OFDM) is widely adopted in broadband wireless signal transmission due to its high spectral efficiency. However, its performance can suffer severely from the intercarrier interference (ICI) induced by fast channel variation resulting from high-speed motion. Such an effect is sometimes referred to as loss of subcarrier orthogonality. The problem becomes increasingly acute as the carrier frequency or the speed of motion increases. For instance, with a 500 km/h mobile speed and a 6 GHz carrier frequency, the peak Doppler frequency can be as high as about 2800 Hz, which translates to over 0.25 times the 10.94 kHz subcarrier spacing in the Mobile WiMAX standard [1]. The signal detection performance can become intolerable without proper countermeasures.

Consider the typical OFDM system illustrated in Fig. 1. In a system without ICI, the channel frequency response matrix that relates the inputs of the inverse discrete Fourier transform (IDFT) and the outputs of the DFT is diagonal. Fast channel variation introduces sizable off-diagonal elements in the matrix, thus resulting in ICI. In theory, an optimal signal detector should take all ICI terms into account. But for reasons of complexity and robustness, usually only the dominant terms are compensated for. As these dominant terms are normally concentrated (circulantly) around the diagonal, the channel matrix shows a (circulant) band structure [2]–[5].

Jeon *et al*. [2] consider the situation where the normalized peak Doppler frequency (i.e., peak Doppler frequency expressed in units of frequency spacing of subcarriers) is on the order of 0.1 or less. In this situation, the channel variation over one OFDM symbol time is approximately linear. A frequency-domain equalizer that exploits the ensuing band channel matrix structure is proposed. Schniter [3] considers substantially higher normalized peak Doppler frequencies, under which the ICI is more widespread. Time-domain windowing is used to partially counteract the effect of channel variation and shrink the bandwidth of the channel matrix. An iterative minimum mean-square error (MMSE) equalizer is then used to detect the signal. Rugini *et al*. [4] employ block-type linear MMSE equalization, wherein the band channel matrix structure is exploited (via triangular factorization of the autocorrelation matrix) to reduce the equalizer complexity. Ohno [5] addresses the ICI via maximum-likelihood sequence estimation (MLSE) in the frequency domain, where the band channel matrix structure is utilized to limit the trellis size.

The consideration of only the dominant ICI terms results in an irreducible error floor in time-varying channels [2]–[5]. Moreover, while the uncompensated residual ICI is colored [6]–[8], for various reasons it is often treated as white [5]–[9]. Although whitening of "I+N" (i.e., sum of ICI and additive channel noise) can lead to improved signal detection performance, it requires knowing the autocorrelation function of I+N, which remains a key problem awaiting solution [7], [8]. Without knowing the autocorrelation function, one can only resort to less sophisticated techniques, such as simple differencing of the received signals at neighboring subcarriers [10]. An attempt to characterize this autocorrelation function for the benefit of signal detection is reported in [11], but a comprehensive understanding of it remains lacking.

The contribution of the present work is twofold. First, we explore the correlation property of ICI and derive an

Manuscript received 29 April 2011; revised 24 October 2011. This work was supported in part by the National Science Council of R.O.C. under Grants NSC 99-2219-E-009-009 and 99-2219-E-009-010. Part of this work was published in [11], IEEE Vehicular Technology Conference, May 2010, Taipei, Taiwan.

The authors are with the Department of Electronics Engineering and Institute of Electronics, National Chiao Tung University, Hsinchu, Taiwan 30010, R.O.C. (e-mails: c93jo6@gmail.com, dwlin@mail.nctu.edu.tw, tzuhsien54120@faculty.nctu.edu.tw).

Digital Object Identifier 10.1109/JSAC.2012.120503.

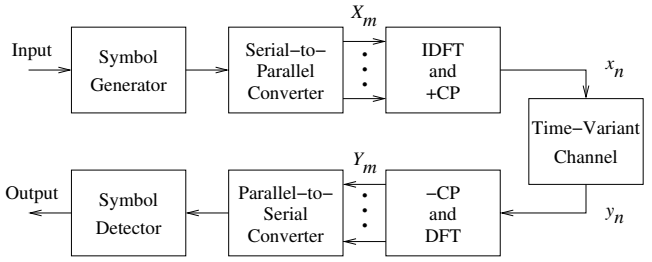

Fig. 1. OFDM system model.

approximate mathematical expression for it. The expression applies not only to classical multipath Rayleigh fading, but also to arbitrary Doppler spectrum shapes in general. It is found that the correlation values are insensitive to various system parameters and channel conditions. Moreover, the correlation values are very high for the residual ICI beyond the few dominant terms. Secondly, to capitalize on the above high correlation to improve signal reception over fast varying channels, we consider performing simple blockwise whitening of the residual I+N before signal detection (i.e., equalization), where the whitener makes use of the ICI characteristics as found. Numerical results show that substantial gains can be achieved with this approach.

The remainder of this paper is organized as follows. Sec. II describes the system model. Sec. III analyzes the correlation property of ICI. Sec. IV introduces the proposed detection method that utilizes the residual ICI's high correlation. It also presents some simulation results. Finally, Sec. V gives a conclusion.

II. System Model

Fig. 1 shows the discrete-time baseband equivalent model of the considered OFDM system. The input-output relation of the channel is given by

$$y_n = \sum_{l=0}^{L-1} h_{n,l} x_{n-l} + w_n \tag{1}$$

where x_n and y_n are, respectively, the channel input and output at time n, L is the number of multipaths, $h_{n,l}$ is the complex gain of the lth path (or tap) at time n, and w_n is the complex additive white Gaussian noise (AWGN) at time n. We assume that the length of the cyclic prefix (CP) is sufficient to cover the length of the channel impulse response (CIR) $(L-1)T_{sa}$, where T_{sa} denotes the sampling period.

One common way of expressing the received signal in the DFT domain is

$$Y_m = \sum_{k=0}^{N-1} \sum_{l=0}^{L-1} X_k H_l^{(m-k)} e^{-j2\pi lk/N} + W_m, \ 0 \le m \le N-1, \tag{2}$$

where X_k and Y_m are, respectively, the channel input and output in the frequency domain (see Fig. 1), N denotes the size of DFT, W_m denotes the DFT of w_m, and $H_l^{(k)}$ is the frequency spreading function of the lth path given by

$$H_l^{(k)} = \frac{1}{N} \sum_{n=0}^{N-1} h_{n,l} e^{-j2\pi nk/N}. \tag{3}$$

Another way of expressing it is

$$\mathbf{y} = \mathbf{H}\mathbf{x} + \mathbf{w} \tag{4}$$

where $\mathbf{y} = [Y_0, ..., Y_{N-1}]'$, $\mathbf{x} = [X_0, ..., X_{N-1}]'$, $\mathbf{w} = [W_0, ..., W_{N-1}]'$, and

$$\mathbf{H} = \begin{bmatrix} a_{0,0} & a_{0,1} & \cdots & a_{0,N-1} \\ a_{1,0} & a_{1,1} & \cdots & a_{1,N-1} \\ \vdots & \vdots & \ddots & \vdots \\ a_{N-1,0} & a_{N-1,1} & \cdots & a_{N-1,N-1} \end{bmatrix}, \tag{5}$$

with $'$ denoting transpose and

$$a_{m,k} = \sum_{l=0}^{L-1} H_l^{(m-k)} e^{-j2\pi kl/N}. \tag{6}$$

The quantity $a_{m,k}$ is the "ICI coefficient" from subcarrier k to subcarrier m. For a time-invariant channel, $H_l^{(k)}$ vanishes $\forall k \neq 0$ and $\mathbf{H}$ becomes diagonal, implying absence of ICI.

As mentioned, a band approximation to $\mathbf{H}$ that retains only the dominant terms about the diagonal may ease receiver design and operation, but also results in an irreducible error floor. Consider a symmetric approximation with one-side bandwidth K, that is, $a_{m,k} = 0$ for $|(m-k)\%N| > K$ where K is a nonnegative integer and $\%$ denotes modulo operation. Then the ICI at each subcarrier consists of contributions from at most $2K$ nearest (circularly) subcarriers. In this work, we exploit the correlation of the residual ICI *outside* the band to attain a significantly enhanced signal detection performance. For convenience, in the following we omit explicit indication of modulo-N in indexing a length-N sequence, understanding an index, say n, to mean $n\%N$.

Let the channel be wide-sense stationary uncorrelated scattering (WSSUS) [12] with

$$E[h_{n,l} h^*_{n-q,l-m}] = \sigma_l^2 r_l(q) \delta(m) \tag{7}$$

where $E[\cdot]$ denotes expectation, σ_l^2 denotes the variance of the lth tap gain, $r_l(q)$ denotes the normalized tap autocorrelation (where $r_l(0) = 1$), and $\delta(m)$ is the Kronecker delta function. For convenience, assume $\sum_l \sigma_l^2 = 1$. Let $P_l(f)$ denote the Doppler power spectral density (PSD) of path l and thus

$$r_l(q) = \left[\int_{-f_d}^{f_d} P_l(f) e^{j2\pi f\tau} df \right] \Bigg|_{\tau = T_{sa} q}, \tag{8}$$

where f_d denotes the peak Doppler frequency of the channel. We assume that the paths may be subject to arbitrary, different fading so that $P_l(f)$ may be asymmetric about $f = 0$ and different for different l.

III. Autocorrelation of Residual ICI

Assume a signal detector (equalizer) able to handle $2K$ terms of nearest-neighbor ICI. We may partition the summation over k in (2) into an in-band and an out-of-band term

as

$$Y_m = \sum_{k=m-K}^{m+K} \sum_{l=0}^{L-1} H_l^{(m-k)} e^{-j2\pi lk/N} X_k + \underbrace{\sum_{k\notin[m-K,m+K]} \sum_{l=0}^{L-1} H_l^{(m-k)} e^{-j2\pi lk/N} X_k}_{\triangleq c_{m,K}} + W_m, \quad (9)$$

where $c_{m,K}$ is the out-of-band term, i.e., residual ICI. Alternatively, using the notation of (6),

$$Y_m = \sum_{k=m-K}^{m+K} a_{m,k} X_k + c_{m,K} + W_m \quad (10)$$

where

$$c_{m,K} = \sum_{k\notin[m-K,m+K]} a_{m,k} X_k. \quad (11)$$

For large enough N, the residual ICI may be modeled as Gaussian by the central limit theorem.

It turns out that the analysis can be more conveniently carried out by way of the frequency spreading functions of the propagation paths than by way of $a_{m,k}$. Hence consider (9). From it, the autocorrelation of $c_{m,K}$ at lag r is given by

$$\begin{aligned} &E[c_{m,K} c_{m+r,K}^*] \\ &= E_s \times \sum_{\substack{k\notin[m-K,m+K] \\ \cup[m+r-K,m+r+K]}} \sum_{l=0}^{L-1} E[H_l^{(m-k)} H_l^{(m+r-k)*}] \\ &= E_s \times \sum_{k\notin[-K,K]\cup[-K-r,K-r]} \sum_{l=0}^{L-1} E[H_l^{(k)} H_l^{(k+r)*}] \end{aligned} \quad (12)$$

where E_s is the average transmitted symbol energy and we have assumed that X_k is white. Invoking (3) and (7), we get

$$\begin{aligned} &E[c_{m,K} c_{m+r,K}^*] \\ &= \frac{E_s}{N^2} \sum_{l=0}^{L-1} \sum_{n=0}^{N-1} \sum_{n'=0}^{N-1} \\ &\qquad \sum_{\substack{k\notin[-K,+K] \\ \cup[-K-r,K-r]}} \sigma_l^2 r_l(n-n') e^{j2\pi[n'(k+r)-nk]/N}. \end{aligned} \quad (13)$$

We show in the Appendix that

$$E[c_{m,K} c_{m+r,K}^*] \approx 4\pi^2 T_{sa}^2 E_s \left(\sum_{l=0}^{L-1} \sigma_l^2 {\sigma_D}_l^2 \right) \rho(K,r,N) \quad (14)$$

where ${\sigma_D}_l^2$ is the mean-square Doppler spread of path l given by ${\sigma_D}_l^2 = \int_{-f_d}^{f_d} P_l(f) f^2 df$ and

$$\rho(K,r,N) = \sum_{\substack{k\notin[-K,K] \\ \cup[-K-r,K-r]}} \frac{1}{(1-e^{-j2\pi k/N})(1-e^{j2\pi(k+r)/N})}. \quad (15)$$

Note that

$$\begin{aligned} &\rho(K,r,N) \\ &= \underbrace{\sum_{k\in[0,N-1]\setminus\{0,-r\}} \frac{1}{(1-e^{-j2\pi k/N})(1-e^{j2\pi(k+r)/N})}}_{\triangleq \rho_0(r,N)} \\ &\quad - \underbrace{\sum_{\substack{k\in[-K,K] \\ \cup[-K-r,K-r] \\ \setminus\{0,-r\}}} \frac{1}{(1-e^{-j2\pi k/N})(1-e^{j2\pi(k+r)/N})}}_{\triangleq \rho_1(K,r,N)}, \end{aligned} \quad (16)$$

where the exclusion of 0 and $-r$ from both ranges of summation is to skip over the points of singularity where the summands are null anyway. Note further that $-1/(1-e^{-j2\pi k/N})$ and $-1/(1-e^{-j2\pi(k+r)/N})$ (as sequences in k) are the DFTs of $[n-(N-1)/2]/N$ and $e^{-j2\pi rn/N}[n-(N-1)/2]/N$ (as sequences in n), respectively. Hence, with Parseval's theorem we get

$$\begin{aligned} \rho_0(r,N) &= \frac{1}{N} \sum_{n=0}^{N-1} \left(n - \frac{N-1}{2} \right)^2 e^{j2\pi rn/N} \\ &= \begin{cases} \frac{N^2-1}{12}, & r=0, \\ \frac{-2}{(1-e^{j2\pi r/N})^2}, & r\neq 0. \end{cases} \end{aligned} \quad (17)$$

For $\rho_1(K,r,N)$, we have

$$\rho_1(K,r,N) = \rho_1^*(K,-r,N), \quad (18)$$

i.e., it is conjugate symmetric in r. Moreover, the summands in the last summation in (16) are symmetric over the range of summation. But the range of summation does not allow us to obtain a compact expression for $\rho_1(K,r,N)$ as that for $\rho_0(r,N)$.

As mentioned, the proposed receiver will whiten the residual I+N before equalization. Here we make some observations of the properties of the normalized autocorrelation of residual ICI, i.e., $E[c_{m,K} c_{m+r,K}^*]/E[|c_{m,K}|^2]$, that are relevant to whitener design and performance. For this, note from (14) that $E[c_{m,K} c_{m+r,K}^*]/E[|c_{m,K}|^2]$ depends only on K and N through $\rho(K,r,N)$; the other factors cancel out. Thus this normalized autocorrelation is independent of the average transmitted symbol energy E_s and the sample period T_{sa}. More interestingly, it is also independent of the power-delay profile (PDP) of the channel (i.e., σ_l^2 vs. l) and the Doppler PSD $P_l(f)$ of each path. While the independence of the normalized autocorrelation on the average transmitted symbol energy may be intuitively expected, its independence of the sample period, the PDP, and the Doppler PSDs of channel paths appears somewhat surprising.

Moreover, the normalized autocorrelation is also substantially independent of the DFT size N. To see this, note that for complexity reason, in a practical receiver both the whitener and the equalizer are likely short. A short equalizer implies a small K and a short whitener implies a small range of r over which the normalized autocorrelation needs to be computed. Hence, when N is large, the exponential functions in the above summations for $\rho_0(r,N)$ and $\rho_1(K,r,N)$ can all be well approximated with the first two terms of their respective

power series expansion (i.e., $e^x \approx 1+x$ when $|x| \ll 1$). As a result, we have

$$\rho(K,r,N) = \rho_0(r,N) - \rho_1(K,r,N) \tag{19}$$

where

$$\rho_0(r,N) \approx \begin{cases} \frac{N^2}{12}, & r=0, \\ \frac{N^2}{2\pi^2 r^2}, & r \neq 0, \end{cases} \tag{20}$$

$$\rho_1(K,r,N) \approx \sum_{k\in[-K,K]\cup[-K-r,K-r]\setminus\{0,-r\}} \frac{N^2}{4\pi^2 k(k+r)}. \tag{21}$$

Thus the normalized autocorrelation, being essentially given by $\rho(K,r,N)/\rho(K,0,N)$, is substantially independent of the DFT size N.

Although the above observations concern ICI only, it is straightforward to extend them to the sum of ICI and AWGN channel noise. In particular, the resulting whitening filter and its performance are also independent of a variety of system parameters and channel conditions, including the DFT size, the sample period, the system bandwidth (which is approximately proportional to the inverse of the sample period), the OFDM symbol period NT_{sa}, the channel PDP, and the Doppler PSDs of the channel paths. They only depend on the ICI-to-noise power ratio (INR) at the receiver. As a result, a whitener parameterized on receiver INR can be designed for all operating conditions, which is advantageous for practical system implementation. (The estimation of ICI and noise powers is outside the scope of the present work. Some applicable methods have been proposed in the literature, e.g., [13] for ICI power and [14] for noise power.)

The whitener performance can be understood to a substantial extent by examining the above approximation to the normalized autocorrelation $E[c_{m,K}c^*_{m+r,K}]/E[|c_{m,K}|^2]$. We leave a detailed study along this vein to potential future work. For now, we shall be content with a first-order understanding by a look at its value at lag $r=1$. A large value indicates that whitening can effectively lower the residual ICI. For this, we see from the above approximation (after some straightforward algebra) that

$$\frac{E[c_{m,K}c^*_{m+1,K}]}{E[|c_{m,K}|^2]} \approx \frac{\rho(K,1,N)}{\rho(K,0,N)} \approx \frac{1-\sum_{k=1}^{K} 1/[k(k+1)]}{\pi^2/6 - \sum_{k=1}^{K} 1/k^2} = \frac{1/(K+1)}{\pi^2/6 - \sum_{k=1}^{K} 1/k^2}. \tag{22}$$

For example, its values for $K=0$–3 are, respectively, 0.6079, 0.7753, 0.8440, and 0.8808, which are substantial indeed.

As a side remark that will be of use later, we note that from (14) and (19), the total ICI power $E[|c_{m,0}|^2]$ can be approximated as

$$\begin{aligned} \sigma^2_{c0} &\triangleq E[|c_{m,0}|^2] \\ &\approx 4\pi^2 T_{sa}^2 E_s \left(\sum_{l=0}^{L-1} \sigma_l^2 {\sigma_D}_l^2 \right) \rho(0,0,N) \\ &\approx \frac{E_s}{12} (2\pi T_{sa} N)^2 \left(\sum_{l=0}^{L-1} \sigma_l^2 {\sigma_D}_l^2 \right), \end{aligned} \tag{23}$$

TABLE I
TWO CHANNEL POWER-DELAY PROFILES USED IN THIS STUDY, WHERE TU6 CORRESPONDS TO THE COST 207 6-TAP TYPICAL URBAN CHANNEL AND SUI4 THE SUI-4 3-TAP CHANNEL

TU6	Tap Index	1	2	3	4	5	6
	Delay (μs)	0.0	0.2	0.5	1.6	2.3	5.0
	Power (%)	19	38	24	9	6	4
SUI4	Tap Index	1	2	3	–	–	–
	Delay (μs)	0.0	1.5	4.0	–	–	–
	Power (%)	64	26	10	–	–	–

which is in essence the upper bound derived in [13]. Moreover, we have an approximation to the partial ICI power beyond the $2K$ central terms as

$$\begin{aligned} \sigma^2_{cK} &\triangleq E[|c_{m,K}|^2] \\ &\approx 4\pi^2 T_{sa}^2 E_s \left(\sum_{l=0}^{L-1} \sigma_l^2 {\sigma_D}_l^2 \right) \rho(K,0,N) \\ &\approx \sigma^2_{c0} \left(1 - \frac{6}{\pi^2} \sum_{k=1}^{K} \frac{1}{k^2} \right). \end{aligned} \tag{24}$$

In the following subsection, we provide some numerical examples to verify the above results on ICI correlation. Then, in the next section, we consider how to incorporate a whitener for residual ICI plus noise in the receiver.

A. Numerical Examples

In this subsection, we verify some key results above by considering two very different channel conditions: multipath Rayleigh fading and simple Doppler frequency shift.

First, consider a multipath channel having the COST 207 6-tap Typical Urban (TU6) PDP as shown in Table I [15, p. 94]. Let the paths be subject to Rayleigh fading with the same peak Doppler frequency f_d, so that $r_l(q) = J_0(2\pi f_d T_{sa} q)$ for all l, where $J_0(\cdot)$ denotes the zeroth-order Bessel function of the first kind [12]. Let the OFDM system have $N = 128$, subcarrier spacing $f_s = 10.94$ kHz, and sampling period $T_{sa} = 1/(Nf_s) = 714$ ns, which are some of the Mobile WiMAX parameters [1].

Figs. 2–4 illustrate the normalized autocorrelation of the residual ICI for $K = 0$–2, respectively, where the theoretical values are calculated using (13). As points of reference, note that a peak Doppler frequency of 1 kHz corresponds to a 180 km/h mobile speed at a 6 GHz carrier frequency, or a 540 km/h mobile speed at a 2 GHz carrier frequency. Figs. 2–4 show that the theory and the simulation results agree well up to very large Doppler spreads. In addition, they also show that, for given lag r, the normalized autocorrelation increases with K. The last fact can be understood by examining (11): as K increases, the residual ICI $c_{m,K}$ is composed of the sum of increasingly fewer terms with generally smaller magnitudes, which naturally leads to higher normalized autocorrelation.

Next, consider a channel with a one-line Doppler PSD equal to $\delta(f - f_d)$; in other words, the channel simply effects a frequency offset of f_d. The temporal autocorrelation of the CIR is given by $r_l(q) = \exp(j2\pi f_d T_{sa} q)$. It turns out that the normalized autocorrelation of residual ICI is very similar to that obtained for the previous example, as the theory predicts.

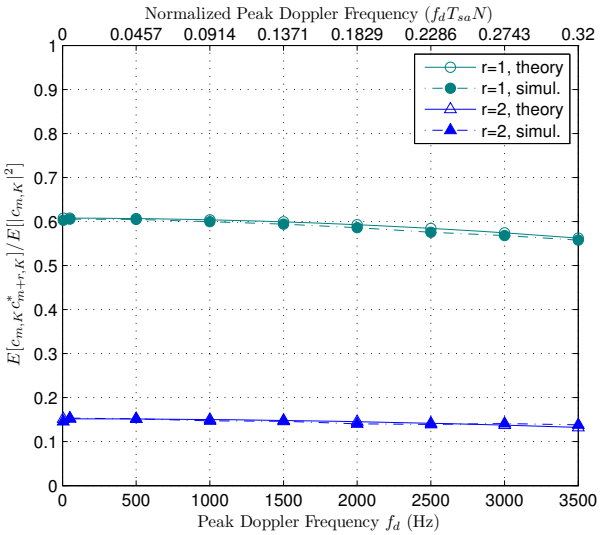

Fig. 2. Normalized autocorrelation of residual ICI over multipath Rayleigh fading channel at $K = 0$, with $N = 128$ and $T_{sa} = 714$ ns. The first-order approximation (19)–(21) yields 0.6079 for $r = 1$ and 0.1520 for $r = 2$, which are quite accurate at low f_d values.

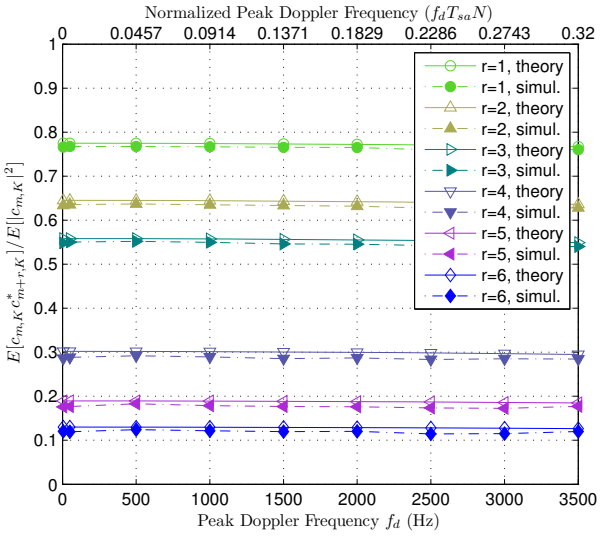

Fig. 3. Normalized autocorrelation of residual ICI over multipath Rayleigh fading channel at $K = 1$, with $N = 128$ and $T_{sa} = 714$ ns. The first-order approximation (19)–(21) yields 0.7753, 0.6461, 0.5599, 0.3036, 0.1912, and 0.1317, for $r = 1$–6, respectively, which are quite accurate.

For space reason, we only illustrate the numerical data for $K = 1$ in Fig. 5, which can be compared with Fig. 3.

Looking backwards from the one-Doppler-line example to the earlier analysis in this Section III, we find that this example also provides an alternative way of interpreting the earlier analytical results. Specifically, an arbitrary Doppler PSD can be considered as composed of a (possibly infinite) number of line PSDs. Hence the autocorrelation of residual ICI associated with an arbitrary Doppler PSD may be obtained as a linear combination of the autocorrelation associated with a line PSD as

$$E[c_{m,K}c^*_{m+r,K}]|_{any\_shape}$$

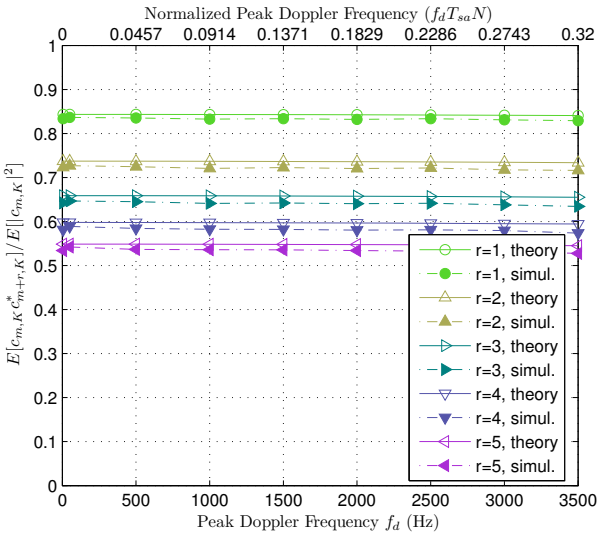

Fig. 4. Normalized autocorrelation of residual ICI over multipath Rayleigh fading channel at $K = 2$, with $N = 128$ and $T_{sa} = 714$ ns. The first-order approximation (19)–(21) yields 0.8440, 0.7358, 0.6612, 0.6014, and 0.5534, for $r = 1$–5, respectively, which are quite accurate.

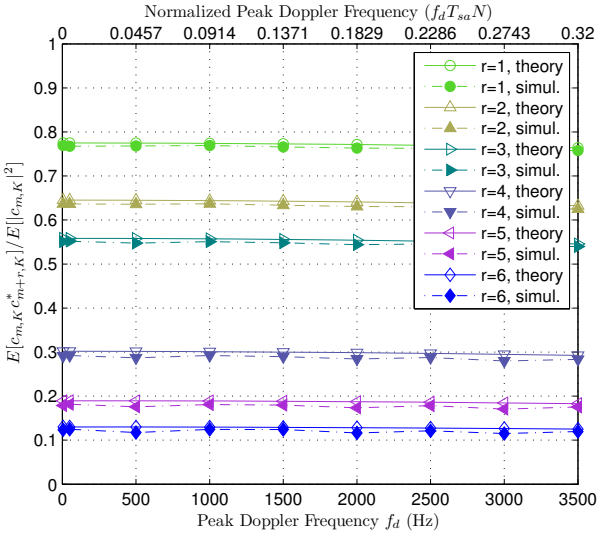

Fig. 5. Normalized autocorrelation of residual ICI over one-Doppler-line channel at $K = 1$, with $N = 128$ and $T_{sa} = 714$ ns.

$$= \sum_{l=0}^{L-1} \sigma_l^2 \int_{-f_d}^{f_d} P_l(f) E[c_{m,K}c^*_{m+r,K}]|_{line,f}\, df \qquad (25)$$

where $E[c_{m,K}c^*_{m+r,K}]|_{any\_shape}$ denotes the autocorrelation of residual ICI associated with a multipath channel of arbitrary Doppler PSD and $E[c_{m,K}c^*_{m+r,K}]|_{line,f}$ that associated with a line Doppler PSD corresponding to a Doppler frequency f. As we have verified now (through Fig. 5, for example) that

$$\frac{E[c_{m,K}c^*_{m+r,K}]|_{line,f_d}}{E[c_{m,K}c^*_{m,K}]|_{line,f_d}} \approx \frac{\rho(K,r,N)}{\rho(K,0,N)}, \qquad (26)$$

substituting it into (25) yields

$$E[c_{m,K}c^*_{m+r,K}]|_{any\_shape}$$
$$\approx \frac{\rho(K,r,N)}{\rho(K,0,N)} \times \sum_{l=0}^{L-1} \sigma_l^2 \int_{-f_d}^{f_d} P_l(f) E[c_{m,K}c^*_{m,K}]|_{line,f}\, df$$

$$= \frac{\rho(K,r,N)}{\rho(K,0,N)} \times E[c_{m,K}c^*_{m,K}]|_{any\_shape}. \quad (27)$$

In other words, since the single-Doppler-line channel shows substantial invariance of the normalized residual ICI autocorrelation over a large range of operating conditions (as we have seen in the last example), it follows that a channel with any Doppler PSD has a similar property.

In summary, we have confirmed that the normalized autocorrelation of the residual ICI is quite insensitive to various system parameters and channel conditions. To lower the error floor, therefore, a whitening filter for the residual ICI plus noise can be designed without regard to these system parameters and channel conditions. Such a fixed design can lead to low implementation complexity and robust performance.

IV. Signal Detection with Whitening of Residual ICI Plus Noise

As indicated, we propose to whiten the residual ICI plus noise in signal detection. This can be applied to many detection methods, including MMSE, iterative MMSE, decision-feedback equalization (DFE), MLSE, etc., providing a wide range of tradeoff between complexity and performance. In this work, we consider an MLSE-based technique both to illustrate how such whitening can be carried out and to demonstrate its benefit. For simplicity, rather than performing whitening over a complete sequence, we do blockwise whitening over windows of size $2q+1$ where q may or may not be equal to K. The details are as follows.

Consider a vector of $2q+1$ frequency-domain signal samples centered at sample m:

$$\mathbf{y}_m = [Y_{m-q} \ \cdots \ Y_m \ \cdots \ Y_{m+q}]' = \mathbf{H}_m\mathbf{x}_m + \mathbf{z}_m \quad (28)$$

where $\mathbf{x}_m = [X_{m-p} \ \cdots \ X_m \ \cdots \ X_{m+p}]'$ for some integer p, $\mathbf{H}_m$ is a $(2q+1)\times(2p+1)$ submatrix of $\mathbf{H}$ of bandwidth K, and $\mathbf{z}_m$ collects all the right-hand-side (RHS) terms in (2) (or (4)) associated with Y_k, $m-q \le k \le m+q$, that do not appear in $\mathbf{H}_m\mathbf{x}_m$. The elements of $\mathbf{z}_m$ include both residual ICI and channel noise. To avoid clogging the mathematical expressions with details, we have omitted explicit indexing of various quantities in (28) with the parameters K, p, and q, understanding that their dimensions and contents depend on these parameters. As examples, with the set of parameters $\{K=1, q=1, p=2\}$, $\mathbf{H}_m$ is given by

$$\begin{bmatrix} a_{m-1,m-2} & a_{m-1,m-1} & a_{m-1,m} & 0 & 0 \\ 0 & a_{m,m-1} & a_{m,m} & a_{m,m+1} & 0 \\ 0 & 0 & a_{m+1,m} & a_{m+1,m+1} & a_{m+1,m+2} \end{bmatrix} \quad (29)$$

whereas with $\{K=1, q=1, p=1\}$, $\mathbf{H}_m$ is given by

$$\begin{bmatrix} a_{m-1,m-1} & a_{m-1,m} & 0 \\ a_{m,m-1} & a_{m,m} & a_{m,m+1} \\ 0 & a_{m+1,m} & a_{m+1,m+1} \end{bmatrix}. \quad (30)$$

Let $\mathbf{K_z} = E[\mathbf{z}_m\mathbf{z}_m^H]$, i.e., the covariance matrix of $\mathbf{z}_m$, where superscript H stands for Hermitian transpose. The aforesaid blockwise whitening of residual ICI plus noise $\mathbf{z}_m$ is given by

$$\widetilde{\mathbf{y}}_m \triangleq \mathbf{K_z}^{-\frac{1}{2}}\mathbf{y}_m = \underbrace{\mathbf{K_z}^{-\frac{1}{2}}\mathbf{H}_m}_{\triangleq\widetilde{\mathbf{H}}_m}\mathbf{x}_m + \underbrace{\mathbf{K_z}^{-\frac{1}{2}}\mathbf{z}_m}_{\triangleq\widetilde{\mathbf{z}}_m} \quad (31)$$

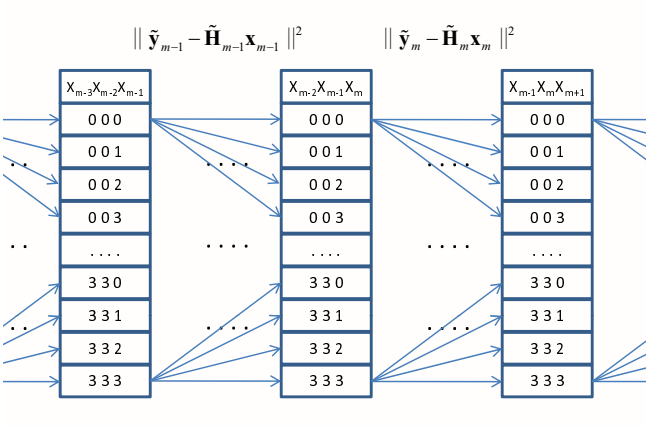

Fig. 6. Trellis structure for MLSE-based detection using the Viterbi algorithm, under QPSK modulation and with $p=1$, where numerals 0–3 represent the QPSK constellation points.

where $\mathbf{K_z}^{-\frac{1}{2}}$ may be defined in more than one way. One choice is to let $\mathbf{K_z}^{-\frac{1}{2}} = \mathbf{U}\mathbf{\Lambda}^{-\frac{1}{2}}\mathbf{U}^H$ where $\mathbf{U}$ is the matrix of orthonormal eigenvectors of $\mathbf{K_z}$ and $\mathbf{\Lambda}$ is the diagonal matrix of corresponding eigenvalues of $\mathbf{K_z}$. If block-by-block signal detection were desired, then the ML criterion would result in the detection rule $\widehat{\mathbf{x}}_m = \arg\min_{\mathbf{x}_m} \|\widetilde{\mathbf{y}}_m - \widetilde{\mathbf{H}}_m\mathbf{x}_m\|^2$. As stated, we consider MLSE-based detection in this work.

In developing the MLSE-based detection method, we treat $\widetilde{\mathbf{z}}_m$, $m=0,\ldots,N-1$, as if they were mutually independent, even though this may at best be only nearly so. Then the probability density function of the received sequence conditioned on the transmitted sequence would be

$$\begin{aligned} &f(\widetilde{\mathbf{y}}_0,\widetilde{\mathbf{y}}_1,\ldots,\widetilde{\mathbf{y}}_{N-1}|\mathbf{x}_0,\mathbf{x}_1,\ldots,\mathbf{x}_{N-1}) \\ &= f(\widetilde{\mathbf{z}}_0,\widetilde{\mathbf{z}}_1,\ldots,\widetilde{\mathbf{z}}_{N-1}) = \prod_{n=0}^{N-1} f(\widetilde{\mathbf{z}}_n). \end{aligned} \quad (32)$$

As a result, the recursive progression of the log-likelihood values, i.e.,

$$\Lambda_k \triangleq \log f(\widetilde{\mathbf{z}}_0,\widetilde{\mathbf{z}}_1,\ldots,\widetilde{\mathbf{z}}_k) = \Lambda_{k-1} + \log f(\widetilde{\mathbf{y}}_k - \widetilde{\mathbf{H}}_k\mathbf{x}_k) \quad (33)$$

(where $k = 1,\ldots,N-1$), leads to a standard Viterbi algorithm. Disregarding some common terms that do not affect sequence detection, in the Viterbi algorithm we may use $\|\widetilde{\mathbf{y}}_k - \widetilde{\mathbf{H}}_k\mathbf{x}_k\|^2$ as the branch metric instead of $\log f(\widetilde{\mathbf{y}}_k - \widetilde{\mathbf{H}}_k\mathbf{x}_k)$. Fig. 6 illustrates the trellis structure of the MLSE detector for $p=1$ under QPSK modulation. A tradeoff between complexity and performance can be achieved by different choices of the three parameters K, q, and p, where p determines the number of states in each trellis stage and the three parameters jointly affect the branch metric structure in the trellis and the autocorrelation structure of the residual ICI (and thereby the whitener behavior).

A. Complexity Analysis

Concerning complexity, let N_A denote the signal constellation size at each subcarrier. Then, for each subcarrier, the nonwhitening MLSE requires $O[(2K+1)N_A^{2K+1}]$ complex multiplications and additions (CMAs) to build the trellis and $O(N_A^{2K+1})$ CMAs to conduct the Viterbi search [5]. In

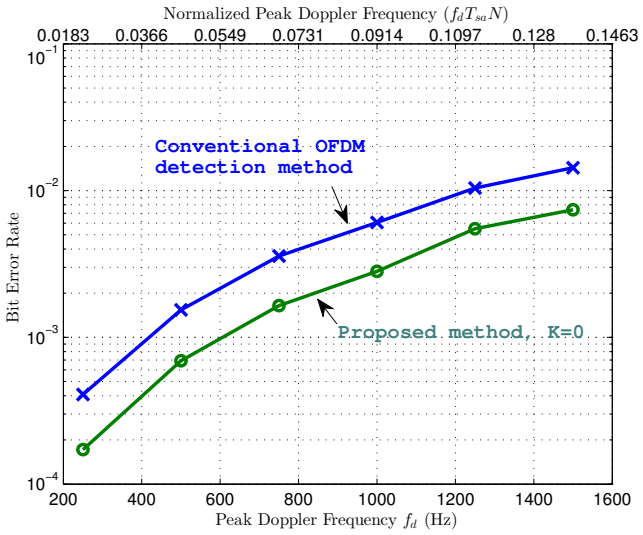

Fig. 7. Error performance in TU6 channel of the conventional OFDM signal detection method and ICI-whitening MLSE (the proposed method) with $K = 0$ and $p = q = 1$ in noise-free condition.

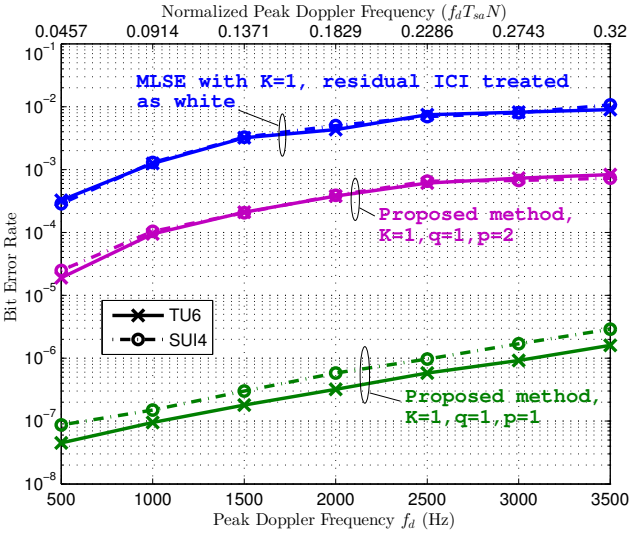

Fig. 8. Comparison of proposed technique in TU6 and SUI4 channels with that treating residual ICI as white; SNR = ∞.

contrast, the proposed method requires $O[(2K+1)N_A^{2p+1} + (2q+1)^2N_A^{2p+1}]$ CMAs to build the trellis, wherein $O[(2K+1)N_A^{2p+1}]$ are for computing $\mathbf{H}_m\mathbf{x}_m$ and $O[(2q+1)^2N_A^{2p+1}]$ are for multiplying with $\mathbf{K_z}^{-\frac{1}{2}}$. Then the Viterbi search requires $O[(2q+1)N_A^{2p+1}]$ CMAs. The computation of $\mathbf{K_z}^{-\frac{1}{2}}$ requires estimation of the ICI power and the AWGN power, but the complexity is far lower than building the trellis or performing the Viterbi search and is thus neglected. From the above, the proposed method may seem to require much higher complexity than nonwhitened MLSE. But, to the contrary, the reduced residual I+N through whitening may facilitate using a smaller ICI bandwidth K in the MLSE, culminating in a complexity gain rather than loss. This will be demonstrated in the simulation results below.

B. Simulation Results on Detection Performance

We present some simulation results on signal detection performance in this subsection. As in Sec. III-A, we let subcarrier spacing $f_s = 10.94$ kHz and sample period $T_{sa} = 714$ ns. The subcarriers are QPSK-modulated with Gray-coded bit-to-symbol mapping. There is no channel coding. The channels are multipath Rayleigh-faded WSSUS channels having the PDPs shown in Table I. Unless otherwise noted, we let $N = 128$ and assume that the receiver has perfect knowledge of the channel state information (CSI), which includes the channel matrix within band K and the covariance matrix $\mathbf{K_z}$ of the residual ICI plus noise.

To start, consider the extreme case of $K = 0$ in absence of channel noise. Through this we look at the limit imposed by the ICI to the performance of the conventional detection method. We also look at the possible gain from blockwise whitening of the full ICI followed by MLSE with $p = q = 1$, at infinite signal-to-noise ratio (SNR). The ICI covariance matrix in this case is given by

$$\mathbf{K_z} = \begin{bmatrix} 1 & 0.6 & 0.15 \\ 0.6 & 1 & 0.6 \\ 0.15 & 0.6 & 1 \end{bmatrix} \sigma_{c0}^2 \tag{34}$$

where recall that $\sigma_{c0}^2 = E[|c_{m,0}|^2]$ is the total ICI power. Fig. 7 shows some simulation results for the TU6 channel. The numerical performance for the SUI4 channel is very similar. These results show that ICI-whitening detection (the proposed technique) yields some advantage over conventional detection: the error probability is reduced by about 2.2 times.

Significantly higher gain can be obtained by ICI-whitening MLSE with $K = 1$. In Fig. 8 we compare the corresponding performance of the proposed technique with that of MLSE which treats the residual ICI as white [5], over TU6 and SUI4 channels in the noise-free condition (i.e., SNR = ∞). For the proposed technique, two parameter settings are considered, viz. $\{q = 1, p = 2\}$ and $\{q = 1, p = 1\}$, for which the covariance matrices $\mathbf{K_z}$ of residual ICI are given by, respectively,

$$\begin{bmatrix} 1 & 0.775 & 0.645 \\ 0.775 & 1 & 0.775 \\ 0.645 & 0.775 & 1 \end{bmatrix} \sigma_{c1}^2, \quad \begin{bmatrix} 1.785 & 1.16 & 1.16 \\ 1.16 & 1 & 1.16 \\ 1.16 & 1.16 & 1.785 \end{bmatrix} \sigma_{c1}^2, \tag{35}$$

where recall that $\sigma_{cK}^2 = E[|c_{m,K}|^2]$ is the residual ICI power outside band K.

Consider the case $p = q = 1$ first. In this case, the proposed method shows a remarkable gain of roughly three to four orders of magnitude in error performance compared to treating residual ICI as white. The error floor induced by the residual ICI can be driven to below 10^{-5} even at the very high normalized peak Doppler frequency of 0.32.

Very interestingly, Fig. 8 also shows that the setting $\{q = 1, p = 2\}$ yields a worse performance than $p = q = 1$, even though the former setting may seem more natural in its associated band channel matrix structure (compare (29) with (30)), which captures all the ICI terms within the modeling range

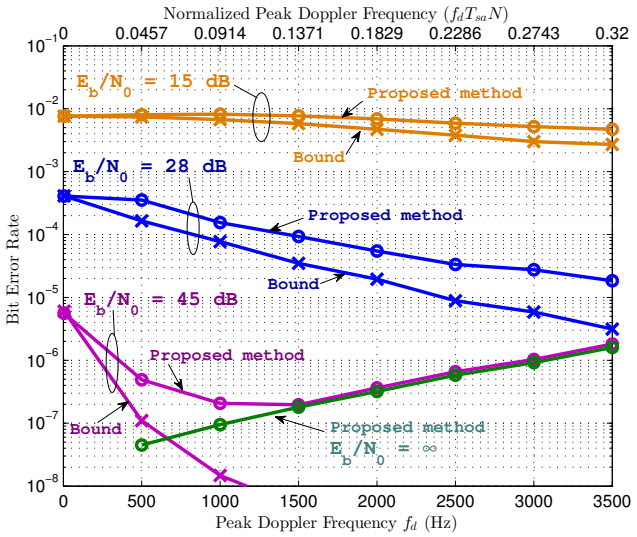

Fig. 9. Performance of proposed technique versus Doppler spread in the TU6 channel with $p = q = K = 1$, at $N = 128$ and $T_{sa} = 714$ ns and under QPSK subcarrier modulation.

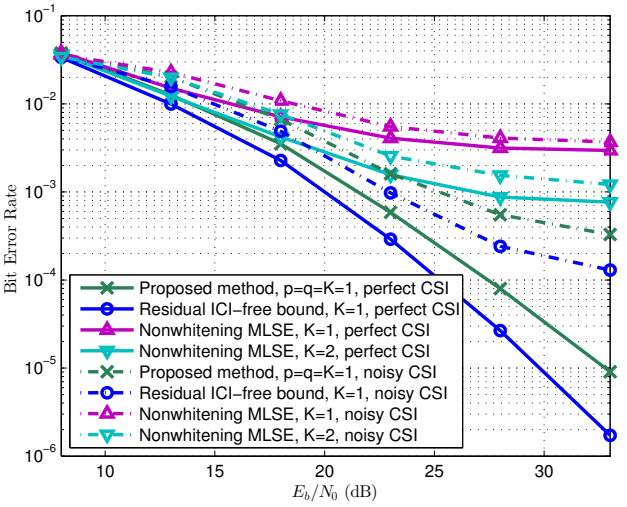

Fig. 10. Performance versus E_b/N_0 of different methods in the TU6 channel, with $N = 128$, $T_{sa} = 714$ ns, $f_d = 1500$ Hz (normalized peak Doppler frequency $f_dT_{sa}N = 0.1371$) and QPSK subcarrier modulation. (Results with $N = 1024$ are very close.)

($K = 1$). Moreover, its corresponding trellis has more states than the latter setting (4^5 vs. 4^3). The reason will be explored in the next subsection. For now, we note that the above results appear to indicate the suitability of setting $p = q = K = 1$ in practical system design. It yields good performance without undue complexity. With this observation, we now present some more simulation results under this setting. The aims are to examine the proposed technique's performance at finite SNR and to compare it with a benchmarking upper bound. For this, we first consider how it varies with Doppler spread and then how it varies with SNR.

Fig. 9 shows some results for the TU6 channel with $p = q = K = 1$ at several SNR values. The results for SUI4 show similar characteristics and are omitted. We compare the performance of the proposed method with a benchmark: the matched-filter bound (MFB), i.e., signal detection with perfect knowledge of the interfering symbols. To make the MFB a more-or-less absolute lower bound, it is obtained with the residual ICI outside band K fully cancelled. Other than these, the same MLSE as in the proposed technique is used. For all three finite SNR values shown, note that the MFB drops monotonically with increasing f_d, i.e., with increasing time-variation of the channel. This is in line with the fact that faster channel variation yields greater time diversity, as various researchers have observed [16]–[18]. However, such time diversity can show clearly only when ICI is sufficiently small (e.g., after ICI cancellation). For the proposed technique, its error performance at $E_b/N_0 = 15$ and 28 dB tracks that of the MFB reasonably closely, deviating by less than a multiplicative factor of three for normalized peak Doppler frequencies up to 0.18 ($f_d \leq 2000$ Hz). At $E_b/N_0 = 45$ dB, the performance improves with f_d until f_d reaches about 1500 Hz (normalized peak Doppler frequency ≈ 0.14). Afterwards, the residual ICI dominates in determining the performance, as can be seen by the closeness between the corresponding curves for $E_b/N_0 = 45$ dB and ∞.

Next, consider how the performance of the proposed method varies with SNR. The solid lines in Fig. 10 show results at $f_d = 1500$ Hz (normalized peak Doppler frequency ≈ 0.14) under perfect CSI. It is seen that the proposed method at $K = 1$ can yield a substantial performance gain compared to nonwhitening MLSE [5] at $K = 2$. The dash-dot lines in Fig. 10 depict some results under imperfect CSI. Limited by space, we cannot elaborate on the many possible channel estimation methods and their performance. Hence the results shown pertain to a typical condition only. For this, we note that the mean-square channel estimation error is typically proportional to the variance of the unestimatable channel disturbance, with the proportionality constant inversely dependent on the sophistication of the channel estimation method [19]. In our case, the unestimatable channel disturbance includes residual ICI (mostly that beyond $K = 1$) and additive channel noise (AWGN). At a normalized peak Doppler frequency of 0.14 ($f_d = 1500$ Hz), the first term is approximately 20 dB below the received signal power. The proportionality constant is set to 1/8. The channel estimation error limits the performance of all detection methods and the residual ICI-free bound in the form of error floors. The floor of the proposed method at $K = 1$ is seen to be lower than that of nonwhitening MLSE at $K = 2$ and is relatively close to the bound. We further note that, while Fig. 10 has been obtained with $N = 128$, the results obtained with $N = 1024$ (eight times the bandwidth) are very close.

C. Dependence of Detection Performance on Parameter Setting

As mentioned, we here explore how signal detection performance depends on whitener parameter setting. In particular, recall that one intriguing phenomenon observed earlier is the worse performance with $p = 2$ than with $p = 1$ (both at $q = K = 1$), although the former is associated with a seemingly more natural-looking band channel matrix and a

more expanded MLSE trellis. A comprehensive analysis would require examining the distance property of the received signal after the proposed blockwise whitening. However, a crude understanding can be obtained by looking at the signal-to-interference-plus-noise ratio (SINR) after blockwise whitening.

From (28) and (31), the pre- and post-whitening SINRs are given by, respectively,

$$\text{SINR}_{pre} = E[\mathbf{x}_m^H \mathbf{H}_m^H \mathbf{H}_m \mathbf{x}_m]/E[\mathbf{z}_m^H \mathbf{z}_m], \quad (36)$$

$$\text{SINR}_{post} = E[\mathbf{x}_m^H \mathbf{H}_m^H \mathbf{K}_\mathbf{z}^{-1} \mathbf{H}_m \mathbf{x}_m]/E[\mathbf{z}_m^H \mathbf{K}_\mathbf{z}^{-1} \mathbf{z}_m]. \quad (37)$$

For the power of residual ICI plus noise, we have $E[\mathbf{z}_m^H \mathbf{z}_m] = \text{tr}(E[\mathbf{z}_m \mathbf{z}_m^H]) = \text{tr}(\mathbf{K}_\mathbf{z})$ and $E[\mathbf{z}_m^H \mathbf{K}_\mathbf{z}^{-1} \mathbf{z}_m] = \text{tr}(E[\mathbf{K}_\mathbf{z}^{-1} \mathbf{z}_m \mathbf{z}_m^H]) = \text{tr}(\mathbf{K}_\mathbf{z}^{-1} \mathbf{K}_\mathbf{z}) = 2q + 1$, where $\text{tr}(\mathbf{A})$ denotes the trace of a matrix $\mathbf{A}$. For the signal power, we have $E[\mathbf{x}_m^H \mathbf{H}_m^H \mathbf{H}_m \mathbf{x}_m] = \text{tr}(E[\mathbf{H}_m^H \mathbf{H}_m \mathbf{x}_m \mathbf{x}_m^H]) = E_s \cdot \text{tr}(E[\mathbf{H}_m^H \mathbf{H}_m]) = E_s \cdot \text{tr}(E[\mathbf{H}_m \mathbf{H}_m^H])$ and $E[\mathbf{x}_m^H \mathbf{H}_m^H \mathbf{K}_\mathbf{z}^{-1} \mathbf{H}_m \mathbf{x}_m] = \text{tr}(E[\mathbf{H}_m^H \mathbf{K}_\mathbf{z}^{-1} \mathbf{H}_m \mathbf{x}_m \mathbf{x}_m^H]) = E_s \cdot \text{tr}(E[\mathbf{H}_m^H \mathbf{K}_\mathbf{z}^{-1} \mathbf{H}_m]) = E_s \cdot \text{tr}(\mathbf{K}_\mathbf{z}^{-1} E[\mathbf{H}_m \mathbf{H}_m^H])$, where E_s is as defined previously (the average energy of the transmitted signal samples) and we have assumed that the transmitted signal is independent and identically distributed (i.i.d.).

Note that the factor $E[\mathbf{H}_m \mathbf{H}_m^H]$ appears in the signal power terms of both SNRs. Employing a procedure similar to that for $E[c_{m,K} c_{m+r,K}^*]$ in Sec. III, we can derive an expression for $E[\mathbf{H}_m \mathbf{H}_m^H]$ in terms of the channel parameters as in the case of $E[c_{m,K} c_{m+r,K}^*]$. However, although such an expression can provide more precise numerical results, an illuminating insight into the SNR impact of the proposed blockwise whitening technique can already be gathered with a very simple approximation to $E[\mathbf{H}_m \mathbf{H}_m^H]$, and this insight is sufficient for the purpose of the present work. Specifically, in the limit of little ICI, $\mathbf{H}_m$ approaches a diagonal matrix of the channel frequency response. In this case, $E[\mathbf{H}_m \mathbf{H}_m^H] \approx (\sum_{l=0}^{L-1} \sigma_l^2)\mathbf{I}$ where $\mathbf{I}$ denotes an identity matrix and recall that we have assumed a unity channel power gain, i.e., $\sum_l \sigma_l^2 = 1$. Hence

$$\text{SINR}_{pre} \approx (2q+1) E_s / \text{tr}(\mathbf{K}_\mathbf{z}), \quad (38)$$

$$\text{SINR}_{post} \approx E_s \cdot \text{tr}(\mathbf{K}_\mathbf{z}^{-1})/(2q+1). \quad (39)$$

As a result,

$$\frac{\text{SINR}_{post}}{\text{SINR}_{pre}} \approx \frac{\text{tr}(\mathbf{K}_\mathbf{z}^{-1}) \cdot \text{tr}(\mathbf{K}_\mathbf{z})}{(2q+1)^2}. \quad (40)$$

Now let λ_i, $0 \le i \le 2q$, denote the eigenvalues of $\mathbf{K}_\mathbf{z}$. Then the eigenvalues of $\mathbf{K}_\mathbf{z}^{-1}$ are given by λ_i^{-1} and we have

$$\frac{\text{SINR}_{post}}{\text{SINR}_{pre}} \approx \frac{(\sum_{i=0}^{2q} \lambda_i^{-1})(\sum_{i=0}^{2q} \lambda_i)}{(2q+1)^2}. \quad (41)$$

Therefore, the more disparate the eigenvalues of $\mathbf{K}_\mathbf{z}$ are, the greater gain the proposed blockwise whitening can offer. If the eigenvalues are all equal, then no gain is attained.

As examples, we consider the previously considered cases 1) $\{K = 0, q = 1, p = 1\}$, 2) $\{K = 1, q = 1, p = 1\}$, and 3) $\{K = 1, q = 1, p = 2\}$, all at infinite SNR. The corresponding $\mathbf{K}_\mathbf{z}$ matrices are given in (34) and (35). For case 1), we obtain the eigenvalues $0.2232\sigma_{c0}^2$, $0.8500\sigma_{c0}^2$, and $1.9268\sigma_{c0}^2$; for case 2), $0.0654\sigma_{c1}^2$, $0.6250\sigma_{c1}^2$, and $3.8796\sigma_{c1}^2$; and for case 3), $0.1800\sigma_{c1}^2$, $0.3550\sigma_{c1}^2$, and $2.4650\sigma_{c1}^2$. The resulting post- to pre-SINR ratios are 2.0588, 8.7052, and 2.9258, respectively. They do correspond monotonically to the performance gains shown in Figs. 7 and 8. However, the mathematical relation between SINR and bit error rate (BER) is not straightforward—a point worth remembering when comparing the SINR performance of different detection methods and different parameter settings.

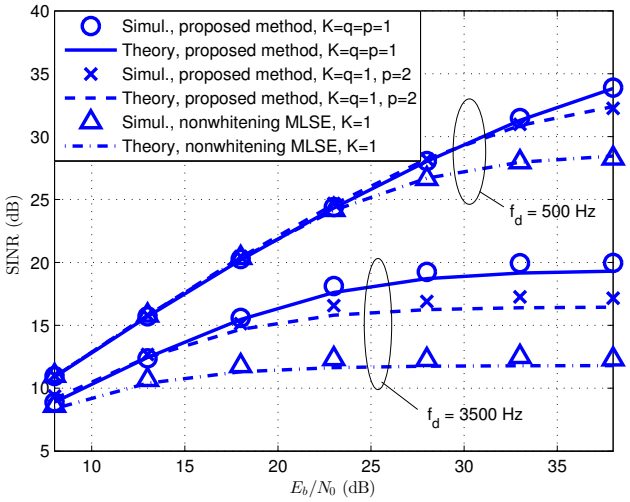

Fig. 11. SINR performance of different methods in the TU6 channel, with $N = 128$ and $T_{sa} = 714$ ns and assuming perfect CSI.

With the above caveat, we show some SINR performance results at finite SNR values in Fig. 11, both to verify the theory derived in this subsection and to further illustrate the performance of different detection methods. In the case of the proposed method, the theoretical SINR values shown in the figure have been obtained using (38) and (39), i.e., $\text{SINR}_{post} = E_s \cdot \text{tr}(\mathbf{K}_\mathbf{z}^{-1})/(2q+1)$, whereas in the case of nonwhitening MLSE, the values of "I" in the theoretical SINR are simply given by σ_{c1}^2, which are calculated using (24) with $K = 1$. We see that, in the case $f_d = 500$ Hz (normalized peak Doppler frequency ≈ 0.046), the theory and the simulation results agree almost exactly, whereas in the case $f_d = 3500$ Hz (normalized peak Doppler frequency ≈ 0.32), the theory consistently underestimates the SINR performance by a fraction of a dB. The latter phenomenon can be understood by the fact that the σ_{c0}^2 as given in (23) is a progressively looser upper bound to the actual ICI power as the normalized peak Doppler frequency increases [13]. The figure confirms the earlier observation concerning the superiority of the proposed method with $K = q = p = 1$, especially in high SNR or high Doppler spread.

V. Conclusion

We found that, in a mobile time-varying channel, the residual ICI beyond several dominant terms had high normalized autocorrelation. We derived a rather precise closed-form approximation for the (unnormalized) autocorrelation function. It turns out that, up to a rather high peak Doppler frequency, the normalized autocorrelation was not sensitive to a variety

of system parameters and channel conditions, including the DFT size, the sample period, the system bandwidth, the OFDM symbol period, the average transmitted symbol energy, the multipath channel profile, and the Doppler PSDs of the channel paths. As a result, a whitening transform for the residual ICI plus noise can be obtained based solely on the ICI-to-noise ratio. Such a transform can be used in association with many different signal detection schemes to significantly improve the detection performance. That it depends only on the ICI-to-noise ratio but no other quantities also implies simplicity and robustness.

We considered MLSE-type signal detection in ICI with blockwise whitening of the residual ICI plus noise. Simulations showed that the proposed technique could attain a substantially lower ICI-induced error floor than conventional MLSE.

APPENDIX
DERIVATION OF (14) AND SOME RELATED COMMENTS

Substituting the inverse Fourier transform relation in (8) into the right-hand side (RHS) of (13), we get

$$\begin{aligned}
&E[c_{m,K}c^*_{m+r,K}] \\
&= \frac{E_s}{N^2}\sum_{l=0}^{L-1}\sum_{n=0}^{N-1}\sum_{n'=0}^{N-1}\sum_{k\notin[-K,+K]\cup[-K-r,K-r]}\sigma_l^2 \\
&\quad\cdot\int_{-f_d}^{f_d}P_l(f)\{\cos[2\pi fT_{sa}(n-n')] \\
&\quad + j\sin[2\pi fT_{sa}(n-n')]\}df\cdot e^{j2\pi[n'(k+r)-nk]/N}. \quad (42)
\end{aligned}$$

Let ξ denote the quantity that collects all the terms associated with $\sin[2\pi fT_{sa}(n-n')]$. That is,

$$\begin{aligned}
\xi &= \frac{E_s}{N^2}\sum_{l=0}^{L-1}\sigma_l^2\int_{-f_d}^{f_d}df P_l(f) \\
&\quad\cdot\sum_{n=0}^{N-1}\sum_{n'=0}^{N-1}\sum_{\substack{k\notin[-K,+K]\\ \cup[-K-r,K-r]}} j\sin[2\pi fT_{sa}(n-n')] \\
&\quad\cdot e^{j2\pi[n'(k+r)-nk]/N}. \quad (43)
\end{aligned}$$

Consider the inner triple sum and denote it by χ. By substituting the variables n, n', and k with ν', ν, and $-(\kappa+r)$, respectively, we get, after some straightforward algebra,

$$\begin{aligned}
\chi &= \sum_{\nu=0}^{N-1}\sum_{\nu'=0}^{N-1}\sum_{\substack{\kappa\notin[-K,+K]\\ \cup[-K-r,K-r]}}\{-j\sin[2\pi fT_{sa}(\nu-\nu')]\} \\
&\quad\cdot e^{j2\pi[\nu'(\kappa+r)-\nu\kappa]/N}. \quad (44)
\end{aligned}$$

A comparison with the inner triple sum in (43) shows that $\chi=-\chi$, which implies $\chi=0$ and thus $\xi=0$. Therefore, only the cosine terms remain in $E[c_{m,K}c^*_{m+r,K}]$. Approximating the cosine function by taking its power series expansion and retaining only up to the second-order term as $\cos x\approx 1-x^2/2$, we get

$$\begin{aligned}
&E[c_{m,K}c^*_{m+r,K}] \\
&\approx \frac{E_s}{N^2}\sum_{l=0}^{L-1}\sigma_l^2\int_{-f_d}^{f_d}P_l(f)df\sum_{\substack{k\notin[-K,K]\\ \cup[-K-r,K-r]}}\underbrace{\sum_{n=0}^{N-1}e^{-j2\pi nk/N}}_{=0} \\
&\quad\cdot\underbrace{\sum_{n'=0}^{N-1}e^{j2\pi n'(k+r)/N}}_{=0} \\
&\quad-\frac{E_s}{2N^2}\sum_{l=0}^{L-1}\sigma_l^2\int_{-f_d}^{f_d}P_l(f)(2\pi fT_{sa})^2df \\
&\quad\cdot\sum_{\substack{k\notin[-K,K]\\ \cup[-K-r,K-r]}}\Bigg[\sum_{n=0}^{N-1}n^2e^{-j2\pi nk/N}\underbrace{\sum_{n'=0}^{N-1}e^{j2\pi n'(k+r)/N}}_{=0} \\
&\quad+\underbrace{\sum_{n=0}^{N-1}e^{-j2\pi nk/N}}_{=0}\sum_{n'=0}^{N-1}n'^2e^{j2\pi n'(k+r)/N} \\
&\quad-2\sum_{n=0}^{N-1}ne^{-j2\pi nk/N}\sum_{n'=0}^{N-1}n'e^{j2\pi n'(k+r)/N}\Bigg] \\
&= 4\pi^2T_{sa}^2E_s\sum_{l=0}^{L-1}\sigma_l^2\int_{-f_d}^{f_d}P_l(f)f^2df \\
&\quad\cdot\sum_{\substack{k\notin[-K,K]\\ \cup[-K-r,K-r]}}\frac{1}{(1-e^{-j2\pi k/N})(1-e^{j2\pi(k+r)/N})}. \quad (45)
\end{aligned}$$

In fact, the above second-order approximation to cosine function is tantamount to assuming linearly time-varying paths in the CIR. To see it, let $h_l(t)$ denote the continuous-time waveform of the lth path of the CIR (of which $h_{n,l}$ is a sampled version) and let $h_l'(t)$ be its time-derivative. Then by a well-known relation between the time-derivative of a stochastic process and its PSD, we have $4\pi^2\sigma_l^2\int P_l(f)f^2df = E\left[|h_l'(t)|^2\right]$ [20, Table 7.5-1]. Therefore, if we approximate the channel by one whose lth path response varies linearly with time in some period with its slope equal to $\left[\overline{|h_l'(t)|^2}\right]^{1/2}$ in magnitude (where the overline in the brackets denotes time average over this period), then the autocorrelation of residual ICI of the approximating channel would be exactly that obtained above, without approximation. In this sense, the second-order approximation to cosine function above is tantamount to assuming linearly time-varying paths in the CIR.

Numerical examples in Section III show that the ensuing approximation to the autocorrelation of the residual ICI is rather accurate even under a relatively large peak Doppler shift.

REFERENCES

[1] IEEE Std. 802.16-2009, *IEEE Standard for Local and Metropolitan Networks — Part 16: Air Interface for Fixed and Mobile Broadband Wireless Access Systems*. New York: IEEE, May 2009.

[2] W. G. Jeon, K. H. Chang, and Y. S. Cho, "An equalization technique for orthogonal frequency-division multiplexing systems in time-variant multipath channels," *IEEE Trans. Commun.*, vol. 47, no. 1, pp. 27–32, Jan. 1999.
[3] P. Schniter, "Low-complexity equalization of OFDM in doubly selective channels," *IEEE Trans. Signal Process.*, vol. 52, no. 4, pp. 1002–1011, Apr. 2004.
[4] L. Rugini, P. Banelli, and G. Leus, "Simple equalization of time-varying channels for OFDM," *IEEE Commun. Lett.*, vol. 9, no. 7, pp. 619–621, July 2005.
[5] S. Ohno, "Maximum likelihood inter-carrier interference suppression for wireless OFDM with null subcarriers," in *Proc. IEEE Int. Conf. Acoust. Speech Signal Process.*, vol. 3, 2005, pp. 849–852.
[6] M. Russell and G. L. Stüber, "Interchannel interference analysis of OFDM in a mobile environment," in *IEEE Veh. Technol. Conf.*, vol. 2, July 1995, pp. 820–824.
[7] A. A. Hutter and R. Hasholzner, "Determination of intercarrier interference covariance matrices and their application to advanced equalization for mobile OFDM," in *Proc. 5th Int. OFDM Workshop*, Hamburg, Germany, Sep. 2000, pp. 33-1–33-5.
[8] A. A. Hutter, J. S. Hammerschmidt, E. de Carvalho, and J. M. Cioffi, "Receive diversity for mobile OFDM systems," in *Proc. IEEE Wirel. Commun. Networking Conf.*, Sep. 2000, pp. 707-712.
[9] S. Ohno and K. A. D. Teo, "Approximate BER expression of ML equalizer for OFDM over doubly selective channels," in *Proc. IEEE Int. Conf. Acoust. Speech Signal Process.*, 2008, pp. 3049–3052.
[10] Y.-H. Yeh and S.-G. Chen, "An efficient fast-fading channel estimation and equalization method with self ICI cancellation," in *Eur. Signal Process. Conf.*, Sep. 2004, pp. 449–452.
[11] H.-w. Wang, D. W. Lin, and T.-H. Sang, "OFDM signal detection in doubly selective channels with whitening of residual intercarrier interference and noise," in *IEEE Veh. Technol. Conf.*, May 2010, pp. 1–5.
[12] W. C. Jakes, *Microwave Mobile Communications*. New York: Wiley, 1974.
[13] Y. Li and L. J. Cimini, Jr., "Bounds on the interchannel interference of OFDM in time-varying impairments," *IEEE Trans. Commun.*, vol. 49, no. 3, pp. 401–404, Mar. 2001.
[14] G. Huang, A. Nix, and S. Armour, "DFT-based channel estimation and noise variance estimation techniques for single-carrier FDMA," in *IEEE Veh. Technol. Conf. Fall*, Sep. 2010, pp. 1–5.
[15] G. L. Stüber, *Principles of Mobile Communication*, 2nd ed. Boston, MA: Kluwer Academic, 2001.
[16] X. Cai and G. B. Giannakis, "Bounding performance and suppressing intercarrier interference in wireless mobile OFDM," *IEEE Trans. Commun.*, vol. 51, no. 12, pp. 2047–2056, Dec. 2003.
[17] D. Huang, K. B. Letaief, and J. Lu, "Bit-interleaved time-frequency coded modulation for OFDM systems over time-varying channels," *IEEE Trans. Commun.*, vol. 53, no. 7, pp. 1191–1199, July 2005.
[18] H.-D. Lin, T.-H. Sang, and D. W. Lin, "BICM-OFDM for cooperative communications with multiple synchronization errors," in *Proc. Int. Wirel. Commun. Mobile Comput. Conf.*, July 2010, pp. 1055–1059.
[19] K.-C. Hung and D. W. Lin, "Pilot-aided multicarrier channel estimation via MMSE linear phase-shifted polynomial interpolation," *IEEE Trans. Wirel. Commun.*, vol. 9, no. 8, pp. 2539–2549, Aug. 2010.
[20] H. Stark and J. W. Woods, *Probability and Random Processes with Applications to Signal Processing*, 3rd ed. Upper Saddle River, New Jersey: Prentice-Hall, 2002.

Hai-wei Wang received the B.S. degree in control engineering and the M.S. degree in electronics engineering from National Chiao Tung University, Hsinchu, Taiwan, R.O.C., in 1995 and 1999, respectively. She was with Silicon Integrated Systems Corp., Hsinchu, during 1999–2002 and with Realtek Semiconductor Corp., Hsinchu, during 2002–2004.

She is currently pursuing the Ph.D. degree in electronics engineering from the National Chiao Tung University. Her research interests are in the areas of digital communications and communication theory.

David W. Lin (S'79-M'81-SM'88) received the B.S. degree in electronics engineering from National Chiao Tung University, Hsinchu, Taiwan, R.O.C., in 1975 and the M.S. and Ph.D. degrees in electrical engineering from the University of Southern California, Los Angeles, CA, U.S.A., in 1979 and 1981, respectively.

He was with Bell Laboratories during 1981–1983 and with Bellcore during 1984–1990 and again during 1993–1994. Since 1990, he has been a Professor with the Department of Electronics Engineering and Institute of Electronics, National Chiao Tung University, except for a leave in 1993–1994. He has conducted research in digital adaptive filtering and telephone echo cancellation, digital subcriber line and coaxial network transmission, speech and video coding, and wireless communication. His research interests include various topics in signal processing and communication engineering.

Tzu-Hsien Sang (S'96-M'00) received the B.S.E.E. degree in 1990 from National Taiwan University and Ph.D. degree in 1999 from the University of Michigan at Ann Arbor. He is currently with the Department of Electronics Engineering and Institute of Electronics, National Chiao Tung University, Taiwan. Prior to joining NCTU in 2003, he had worked in Excess Bandwidth, a start-up company at Sunnyvale, California, working on physical layer design for broadband technologies. His research interests include signal processing for communications, time-frequency analysis for biomedicl signals, and RF circuit noise modeling.